PAPER

Linear analysis of bump on tail instability with non-Maxwellian distribution function

Plasma Research Express

PAPER

Linear analysis of bump on tail instability with non-Maxwellian distribution function

N Noreen[1], A Shiekh[1,2], I Habumugisha[3,4], S Zaheer[1] and H A Shah[1]

[1] Forman Christian College (A Chartered University), Ferozpur Road, Lahore 54600, Pakistan
[2] Government College Women University, Sialkot 51310, Pakistan
[3] Department of Physics, Kabale University, Kabale, 317, Uganda
[4] Department of Physics, Islamic University in Uganda, Mbale, 2555, Uganda

E-mail: nailanoreen@fccollege.edu.pk

RECEIVED
30 October 2019

REVISED
21 March 2020

ACCEPTED FOR PUBLICATION
28 April 2020

PUBLISHED
7 May 2020

Keywords: solar wind, Instability, Growth rate

Abstract

The growth rate of bump on tail instability propagating in unmagnetized plasma has been derived. The dispersion relation has been characterized for (r, q) distribution function with spectral indices r and q which ultimately contributes towards tails and shoulder of distribution function. The growth rate of the bump on tail instability has been estimated numerically for different ratios of temperature and number density using solar wind data and also by varying values of indices r and q . The higher value of q play the role towards decreasing the growth rate where the instability has the higher value when the number density of the superthermal electrons in the bump is higher and the temperature is low. The maximum growth rate increases with the increase in number density of electrons and decreases with the increasing temperature in the bump.

1. Introduction

'Bump on tail' is a microinstability generated when an electron beam is injected into plasma, as a consequence of which the particle velocity distribution function gets a 'bump' on its 'tail'. Initially Filbert *et al* [1], and Papadopoulos *et al* [2] discussed this idea but both were unable to explain the stabilization of the beam at low energies. Later, Freund *et al* [3] discussed the more general schemes of beam stabilization in the presence of superthermal background solar wind electrons which is more relevant to the actual circumstances of the foreshock.

A modified concept of bump-on-tail instability saturation was proposed by Klimas *et al* [4] in the Earth's foreshock regime. With the help of numerical simulation and quasi-linear analysis they argued that the Filbert's mechanism is also operative during the evolution of the bump-on-tail instability. The saturated plasma state represents a balance between its creation mechanism and velocity space diffusion and cannot determined by velocity space diffusion alone.

Fitzenreiter *et al* [5] derived three-dimensional measurements of velocity distribution of electrons in the 7eV to 500 eV range for the electron foreshock. Schmit *et al* [6] discussed the bump on tail instability through particle-in-cell simulations. Their analysis includes the evolution of the bump-on-tail instability for plasma subject to one-dimensional mechanical compression.

Valentini *et al* [7] used the toy model for resonant wave particle interaction in an unmagnetized plasma. They captured the linear growth of bump on tail instability and particle trapping effects which produce the saturation of the instability and drive the non linear phase of wave particle interaction.

Maxwellian distribution is the natural distribution in case of thermodynamic equilibrium. However observed distribution functions in space and laboratory plasmas, show a significant deviation from the Maxwellian distribution function. Data analysis prove that natural space environment such as chromosphere, solar wind, solar corona, magnetosheath, magnetosphere and astrophysical plasma contains particles which exhibit high energy tails that lead to non-Maxwellian distributions.

The electron velocity distribution function in space is observed to be non-Maxwellian and that is widely confirmed by the data collected from spacecraft [8]. Such non-Maxwellian distributions can be responsible for a lot of different characteristics of plasma waves and instabilities. The increase in energy leads to the formation of high energy tails which can be more precisely described by Lorentzian Kappa (κ) distribution function or may be expressed in power law form as generalized (r, q) distribution function. Such kind of deviations occur when plasma is moderately collisional. Lorentzian Kappa distribution is a convenient mathematical choice to study weakly collisional plasmas [9, 10]. The general (r, q) distribution function is given by [11–13] ,

$$f(r,\,q) = \frac{3(q-1)^{\frac{-3}{2+2r}}\Gamma(q)}{4\pi\Psi_{\perp}^{2}\Psi_{\parallel}\Gamma\left(q-\frac{3}{2+2r}\right)\Gamma\left(1+\frac{3}{2+2r}\right)}\left(1+\frac{1}{q-1}\left(\left(\frac{v_{\parallel}}{\Psi_{\parallel}}\right)^{2}+\left(\frac{v_{\perp}}{\Psi_{\perp}}\right)^{2}\right)^{r+1}\right)^{-q} \tag{1}$$

where r and q are the spectral indices and Ψ is the thermal speed related to particle termal velocity emerges from the definition of the temperature for distribution function. $f(r, q)$ has been normalized such that $\int f(r,\,q)d^{3}v \;=\; 1.$

$$\Psi_{\parallel} = \frac{T_{\parallel}}{m} \times \sqrt{\frac{3(q-1)^{\frac{-1}{1+r}}\Gamma\left(q-\frac{3}{2+2r}\right)\Gamma\left(\frac{3}{2+2r}\right)}{\Gamma\left(\frac{5}{2+2r}\right)\Gamma\left(1+\frac{5}{2+2r}\right)}}$$

and

$$\Psi_{\perp} = \frac{T_{\perp}}{m} \times \sqrt{\frac{3(q-1)^{\frac{-1}{1+r}}\Gamma\left(q-\frac{3}{2+2r}\right)\Gamma\left(1+\frac{3}{2+2r}\right)}{\Gamma(q-\frac{5}{2+2r})\Gamma\left(1+\frac{5}{2+2r}\right)}}$$

Γ is the normal Gamma Function.

In figure 1, there is a comparison of normalized (r, q) distribution function and Maxwellian distribution function. The dashed line shows the Maxwellian distribution function and colored lines show the behavior of (r, q) distribution function. The (r, q) distribution reduces to Maxwellian for $q \to \infty$ and $r = 0$. If the value of q increases taking r fixed as in figure 1(a), the contribution of high energy particles increases with the shrinkage of the shoulder of the distribution function [14, 11, 12, 15]. On the other hand, If the value of r increases, taking the value of q fixed, the contribution of high energy particles is reduced and the shoulder in the distribution function is broadened. It is also observed that the contribution of high energy particles increases with increasing number density of electrons in the unstable region with the fact that temperature of the electrons is low. The (r, q) distribution function is the generalized form of kappa distribution function and reduces to kappa distribution function with r $= 0$ limit. This distribution function is common in both natural and laboratory plasmas i.e., shock waves, solar wind, magnetotails etc. Data analysis for solar wind plasma suggests the superiority of (r, q) distribution function over the simple kappa distribution function [16, 17].

According to the problem, the modified one dimensional (r, q) velocity distribution function for electrons can take the form with bump in it,

$$\begin{aligned} f_{e0}(v_z) = {} & \frac{n_1}{n_e}\frac{\Gamma(q)(q-1)^{\frac{-1}{2+2r}}}{2\Psi_1\Gamma\left(q-\frac{1}{2+2r}\right)\Gamma\left(1+\frac{1}{2+2r}\right)}\left(1+\frac{1}{q-1}\left(\frac{v_z^2}{\Psi_1^2}\right)^{r+1}\right)^{-q} \\ & + \frac{n_2}{n_e}\frac{\Gamma(q)(q-1)^{\frac{-1}{2+2r}}}{4\Psi_2\Gamma\left(q-\frac{1}{2+2r}\right)\Gamma\left(1+\frac{1}{2+2r}\right)} \\ & \left[\left(1+\frac{1}{q-1}\left(\frac{(v_z-v_o)^2}{\Psi_2^2}\right)^{r+1}\right)^{-q}+\left(1+\frac{1}{q-1}\left(\frac{(v_z+v_o)^2}{\Psi_2^2}\right)^{r+1}\right)^{-q}\right] \end{aligned} \tag{2}$$

where n_1 is number density of thermal region and n_2 is for bump region and $n_e = n_1 + n_2$, where T_1, T_2 are the temperature of the electrons of thermal and bump regions respectively, where the thermal velocities are

$$\Psi_1 = \sqrt{\frac{T_1}{m_e}} \times \sqrt{\frac{3(q-1)^{\frac{-1}{1+r}}\Gamma\left(q-\frac{1}{2+2r}\right)\Gamma\left(1+\frac{1}{2+2r}\right)}{\Gamma\left(q-\frac{3}{2+2r}\right)\Gamma\left(1+\frac{3}{2+2r}\right)}}$$

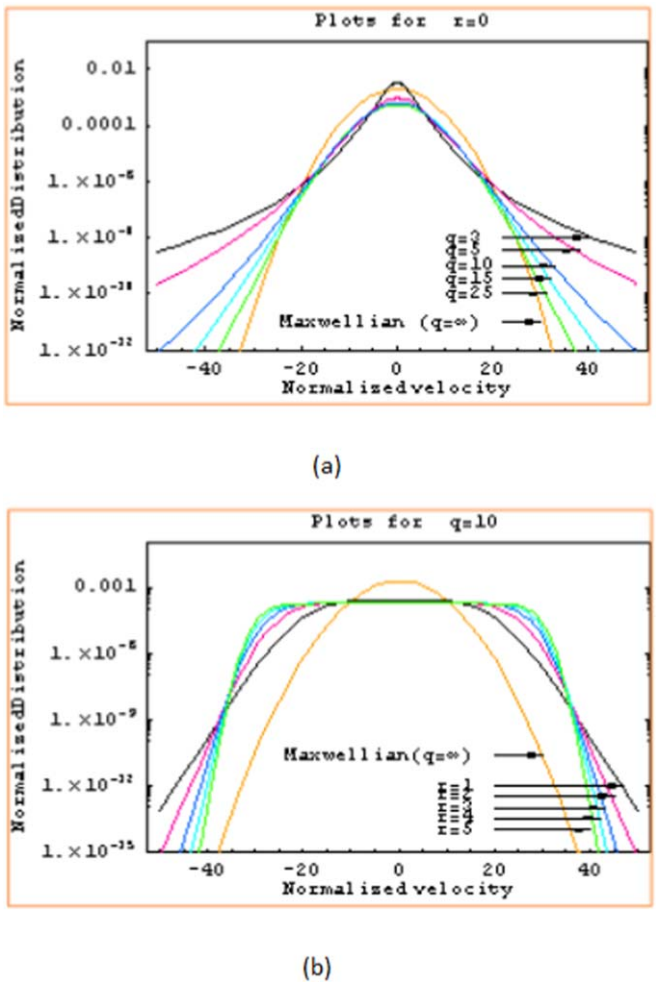

Figure 1. The (a) part shows behavior of distribution function with different values of index q when index r is fixed and part (b) shows fixed value of index q while r varies.

and

$$\Psi_2 = \sqrt{\frac{T_2}{m_e}} \times \sqrt{\frac{3(q-1)^{\frac{-1}{1+r}}\Gamma\left(q-\frac{1}{2+2r}\right)\Gamma\left(1+\frac{1}{2+2r}\right)}{\Gamma\left(q-\frac{3}{2+2r}\right)\Gamma\left(1+\frac{3}{2+2r}\right)}}$$

The (r, q) distribution function fits with the data obtained form the AMPTE satellite for magnetosheath and the solar wind data collected from the CLUSTER [16]. Qureshi *et al* [18] investigated the parallel propagation of waves in general and Alfven waves in particular by using the (r, q) distribution function. The new dispersion relation was derived and its properties were widely studied. The Landau damping of the Langmuir waves with the reduction in the spectral indices r and q was studied in detail in hot, isotropic, unmagnetized plasma [19]. Linear stability analysis of (r, q) distribution with Whistler wave and its comparison with CLUSTER data leads to the good agreement both quantitatively and qualitatively [14]. Zaheer *et al* [11] presented a realistic picture of perpendicularly propagating electromagnetic modes i.e, O-mode and X-mode in strongly magnetized hot plasma by using (r, q) distribution function. Zaheer *et al* [12] also calculated the Weibel instability in unmagnetized plasma by non-Maxwellian distribution function. The solar wind electrons were modeled by Zaheer and Yoon by using (r, q) distribution near 1 AU[13]. Hashemzadah [20] has used the q-nonextinsive distributive function for calculation of eigenmodes of filamentation instability. In his manuscript, he calculated the growth rate of filamenattion instability dependence on electron velocity and q-nonextensive parameter. According to [20], both factors play the same role to deal with growth rate. As we are dealing with the generalized (r, q) distribution function and studied the dependence of growth rate on r and q indices seperatly. So in both caseas, we obsreved the growth rate is maximum at higher r values and decreases with the increase in the value of q.

In section 1, we have introduced the modified (r, q) distribution keeping in mind that it better fits with the solar wind data especially when there is a presence of high energy tails and indication of formation of shoulders

and bumps in the distribution function. In section 2, by using kinetic theory the dispersion relation of the bump on tail instability has been derived. Relying on that dispersion relation we have further calculated the analytical expressions for growth rate and the maximum growth rate of the instability. In section 3, we have discussed the results based on the numerical analysis from the solar wind data.

2. Mathematical model

In this manuscript, a beam of high energy electrons of velocity v_0 has been introduced in the z-direction, in (r, q) velocity distribution. The electron beam produces a relative velocity $(v_z - v_0)$ and $(v_z + v_0)$ in the positive as well as in negative z-direction respectively. The ions being massive are assumed to form a fixed background. The distribution is considered to be symmetric in order to neglect the effects of current as this is a microinstability and falls in the category of electrostatic instability [15]. The plasma oscillations are characterized by $D(k, \omega) = 0$, where the frequency consists of real as well as imaginary part. If $\omega = \omega_r + i\omega_i$, then ω_r is the real frequency and ω_i is the imaginary part of frequency. So in $D(k, \omega) = D_r(k, \omega_r) + iD_i(k, \omega_r)$, the real part of $D_r(k, \omega_r)$ tells us about the behavior of the plasma to electric field which is generated in the plasma wave. While the damping or growth rate is characterized by ω_i which explains that the particles are in resonance with disturbance. The real frequency ω_r in isotropic plasma can be written as [21]

$$D_r(k, \omega_r) = 1 - \frac{\omega_{P_e}^2}{k^2} \int_{-\infty}^{\infty} \frac{\frac{\partial f_{e0}}{\partial v}}{v - \frac{\omega_r}{k}} dv = 0 \tag{3}$$

$$D_i = -\frac{\pi \omega_{P_e}^2}{k^2} \left(\frac{\partial f_{e0}}{\partial v} \right)_{v=\frac{\omega_p}{k}} \tag{4}$$

As we have taken ions form neutralizing background, the plasma frequency will be for electrons only given as $\omega_{pe} = \left(\frac{4\pi e^2 n_e}{m_e}\right)^{\frac{1}{2}}$

The imaginary component of D i.e., D_i is used to compute the growth or damping rates

$$\omega_i = \frac{-D_i(k, \omega_r)}{\partial D_r(k, \omega_r)/\partial \omega_r} \tag{5}$$

By taking derivative of equation (2) and substituting into equation (3), we get expression for electron plasmawave i. e., Langmuir wave

$$D_r = 1 - \frac{\omega_{pe}^2}{\omega_r^2} - \frac{3\omega_{pe}^2}{\omega_r^4} k_z^2 \frac{T_1}{m} \tag{6}$$

assuming the conditions $n_1 \gg n_2$, $n_1 T_1 \gg n_2 m_e v_0^2$ for real part,

$$D_r = 1 - \frac{\omega_{p1}^2}{\omega_r^2} - \frac{3\omega_{p1}^4}{\omega_r^4} k_z^2 \lambda_{D1}^2 \tag{7}$$

It must be clear that ω_{pe} is electron plasma frequency while ω_{p1} is frequency of electrons in thermal region. And $\omega_{p1}^2 = \frac{4\pi n_1 e^2}{m_e}$. Making $D_r = 0$,we can reproduce the standard results as $\omega_r^2 = \omega_{p1}^2(1 + 3k_z^2 \lambda_{D_1}^2)$. Where $\lambda_{D_1}^2 = \frac{T1}{4\pi n_1 e^2}$. It is quite clear from the above equation that real frequency of the langmuir wave has not changed due to the presence of bump in the velocity distribution function. It is also noted that the real frequency is same as when a single bump is present in Maxwellian plasma. The real frequency of Langmuir waves does not change in the presence of superthermal electrons.

The imaginary part of distribution function by assuming the same conditions as for the real part turns to be

$$D_i = \frac{\pi \omega_{pe}^2}{k^2} \frac{\Gamma(q+1)(1+r)(q-1)^{-\frac{3+2r}{2+2r}}}{\Gamma\left(q - \frac{1}{2+2r}\right)\Gamma\left(1 + \frac{1}{2+2r}\right)} \left[\frac{n_1}{n_e} \frac{1}{\Psi_1^2} \alpha + \frac{n_2}{n_e} \frac{1}{2\Psi_2^2} (\beta + \gamma) \right] \tag{8}$$

where $\alpha = \left(\frac{\omega_r / k_z}{\Psi_1}\right)^{2r+2} \left(1 + \frac{1}{q-1} \left(\frac{\omega_r / k_z}{\Psi_1}\right)^{2r+2}\right)^{-1-q}$

$\beta = \left(\frac{\omega_r / k_z - v_o}{\Psi_2}\right)^{2r+2} \left(1 + \frac{1}{q-1} \left(\frac{\omega_r / k_z - v_o}{\Psi_2}\right)^{2r+2}\right)^{-1-q}$

and $\gamma = \left(\frac{\omega_r / k_z + v_o}{\Psi_2}\right)^{2r+2} \left(1 + \frac{1}{q-1} \left(\frac{(\omega_r / k_z + v_o)}{\Psi_2}\right)^{2r+2}\right)^{-1-q}$

Differentiating equation (7), we get

$$\frac{\partial D_r}{\partial \omega_r} = \frac{2\omega_{p_1}^2}{\omega_r^3} + 12k_z^2\lambda_{D_1}^2\frac{\omega_{p_1}^4}{\omega_r^5} \tag{9}$$

By substituting D_i and $\partial D_r/\partial\omega_r$ from equation (9) and equation (10) into equation (5), the following growth rate is obtained under approximations $n_1 \gg n_2$, $T_1 \gg T_2$ and $k_z\lambda_{D_1} \ll 1$,

$$\omega_i = \frac{\sqrt{\pi}\omega_{p1}}{k_z^3\lambda_{D_1}^3}\frac{\Gamma(q+1)}{\Gamma\left(q-\frac{1}{2}\right)(2q-3)^{\frac{3}{2}}} \left[\frac{n_2}{n_1}\left(\frac{T_1}{T_2}\right)^{\frac{3}{2}}\left(\frac{k_z v_o}{\omega_r}-1\right)\left(1+\frac{T_1/T_2}{k_z^2\lambda_{D_1}^2(2q-3)}\left(1-\frac{k_z v_o}{\omega_r}\right)^2\right)^{-1-q} - \left(1+\frac{1}{k_z^2\lambda_{D_1}^2(2q-3)}+\frac{3}{(2q-3)}\right)^{-1-q}\right] \tag{10}$$

The first part of the equation tells about the contribution of positive part of tail of distribution function. The second term of right hand side shows the Landau damping of the wave. The negative tail of the distribution has been ignored because of the significance of the position of the observer in instability criteria. The growth rate of 'bump on tail' instability for the (r, q) distribution function and is maximum when $r = 0$, turns out to be instability condition

$$\left|\frac{k_z v_o}{\omega_r}\right| = 1 + \sqrt{\frac{2q-3}{q+1}}\sqrt{\frac{T_2}{T_1}}k_z\lambda_{D_1} \tag{11}$$

which under approximation $k_z\lambda_{D_1} \ll 1$ leads to $k_z \approx \frac{\omega_{p1}}{v_0}$. Under these approximations ω_{p1} can be used in place of ω_r. Considering all these conditions the maximum growth rate becomes

$$\omega_{i\,\max} = \frac{\sqrt{\pi}\omega}{k_z^3\lambda_{D_1}^3}\frac{\Gamma(q+1)}{\Gamma\left(q-\frac{1}{2}\right)(2q-3)^{\frac{3}{2}}}\left[\frac{n_2}{n_1}\frac{T_1}{T_2}\sqrt{\frac{2q-3}{q+1}}\frac{m_e v_o^2}{T_1}k_z^3\lambda_{D_1}^3\left(\frac{q+2}{q+1}\right)^{-1-q} - \left(1+\frac{1}{k_z^2\lambda_{D_1}^2(2q-3)}+\frac{3}{(2q-3)}\right)^{-1-q}\right] \tag{12}$$

The above equation clearly depends upon q and other plasma parameters. Therefore, it comes to the understanding that the instability gains maximum value at $k_z \approx \frac{\omega_{p1}}{v_0}$, and propagates in parallel direction to the particle velocity in the bump.

In case of $r = 1$, the growth rate is maximum under the following instability condition

$$\left|\frac{k_z v_o}{\omega_r}\right| = 1 + \sqrt{\frac{3\Gamma\left(q-\frac{1}{4}\right)\Gamma\left(\frac{5}{4}\right)}{(q+1)\Gamma\left(q-\frac{3}{4}\right)\Gamma\left(\frac{7}{4}\right)}}\sqrt{\frac{T_2}{T_1}}k_z\lambda_{D_1} \tag{13}$$

The maximum growth rate will then be

$$\omega_{i\,\max} = \frac{\pi\omega_{p1}\,\Gamma(q+1)}{3}\left(\frac{\Gamma\left(q-\frac{3}{4}\right)\Gamma\left(\frac{7}{4}\right)}{3\Gamma\left(q-\frac{1}{4}\right)\Gamma\left(\frac{5}{4}\right)}\right)\left[\frac{n_2}{n_1}\frac{T_1}{T_2}\frac{m_e v_o^2}{T_1}\frac{q}{(q+1)} - \frac{1}{k_z^3\lambda_{D_1}^3}\frac{\Gamma\left(q-\frac{3}{4}\right)\Gamma\left(\frac{7}{4}\right)}{\sqrt{3}\left(\Gamma\left(q-\frac{1}{4}\right)\Gamma\left(\frac{5}{4}\right)\right)^2}\left(1+\frac{1}{3k_z^2\lambda_{D_1}^2}\right)\left\{1-\frac{q+1}{k_z^2\lambda_{D_1}^2}\left(\frac{\Gamma\left(q-\frac{3}{4}\right)\Gamma\left(\frac{7}{4}\right)}{\Gamma\left(q-\frac{1}{4}\right)\Gamma\left(\frac{5}{4}\right)}\right)^2\left(1+\frac{1}{3k_z^2\lambda_{D_1}^2}\right)^2\right\}\right] \tag{14}$$

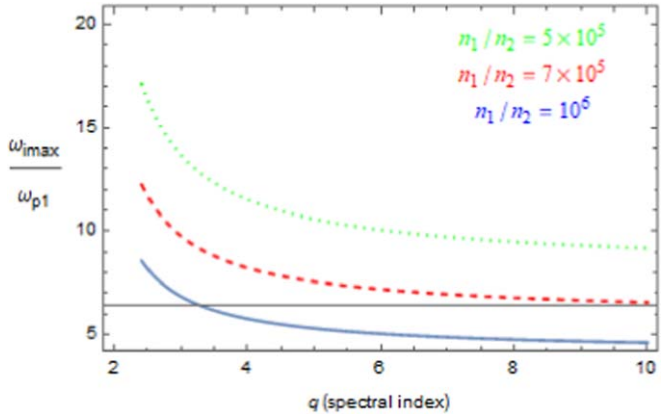

Figure 2. The Growth rate vs q (spectral index) for $n_1/n_2 = 5 \times 10^5$, 7×10^5, 10^6 and $T_1/T_2 = 500$ where r $= 0$.

The growth rate will be maximum when $r = 2$, where we obtain the following instability condition

$$\left| \frac{k_z v_o}{\omega_r} \right| = 1 + \sqrt{\frac{6\Gamma\left(q-\frac{1}{6}\right)\Gamma\left(\frac{7}{6}\right)}{\left(\Gamma\left(q-\frac{1}{2}\right)\sqrt{\pi}\right.}} \sqrt{\frac{T_2}{T_1}} \frac{k_z \lambda_{D_1}}{(q+1)^{\frac{1}{3}}} \tag{15}$$

The maximum growth rate will then be

$$\omega_{i\,\max} = \frac{\pi\omega_{p1}\Gamma(q+1)}{2\sqrt{2}} \frac{\left(\Gamma\left(q-\frac{1}{2}\right)\Gamma\left(\frac{1}{2}\right)\right)^2}{\left(\Gamma\left(q-\frac{1}{6}\right)\Gamma\left(\frac{7}{6}\right)\right)^3} \left[\frac{n_2}{n_1}\frac{T_1}{T_2}\frac{m_e v_o^2}{T_1}\frac{q}{(q+1)^{8/3}} - \frac{\Gamma\left(q-\frac{1}{2}\right)\Gamma\left(\frac{1}{2}\right)}{2k_z^2\lambda_{D_1}^2}\left(1+\frac{1}{3k_z^2\lambda_{D_1}^2}\right) \left\{1+\frac{(q+1)k_z\lambda_{D_1}}{6}\left(1+\frac{1}{3k_z^2\lambda_{D_1}^2}\right)^3 \frac{\Gamma\left(q-\frac{1}{2}\right)\Gamma\left(\frac{1}{2}\right)}{\Gamma\left(q-\frac{1}{6}\right)\Gamma\left(\frac{7}{6}\right)}\right\}\right] \tag{16}$$

The above equations clearly show the dependence of maximum growth rate at different values of r and q and other plasma parameters. Also the unstable wave propagates in z-direction which is parallel to velocity of particle in bump also present in the distribution.

3. Numerical analysis

We have used the values of number density and temperature $n_e = 8.7 \times 10^6 m^{-3}$ and $T_1 = 2 \times 10^5 K$ respectively for analysis [22, 23], which satisfies the solar wind regime. Bukhari *et al* [24] discussed the kinetic instability in the same region i.e; solar wind, where the temperature and number density is same as in the present manuscript. That is a good evidence of presence of kinetic instabilities in solar wind regime. The number density and temperature of the particles in the bump of the tail are chosen under the limiting conditions as used in the calculations i.e. $n_1 \gg n_2$, $n_1 T_1 \gg n_2 m_e v_0^2$, and the value of $k_z \lambda_{D1}$ is considered to be 10^{-3}. The velocity distribution function of such particles is considered to be quasilinear treated by generalized Maxwellian function with mean thermal velocities whereas non maxwellian tails are treated by Lorentzain Kappa distribution function due to high energy tails and large thermal velocities of electrons towards tails. Such deviations from normal behavior have already been identified in literature with Kappa distribution function [25]. The real frequency ω_r is independent of the index (r) as observed by equation (14). However, the growth rate and its maximum value depends upon q and it is clearly observed by equations (13), (15) and 16. In the limit of $r = 0$ and $q = \kappa + 1$ the (r, q) distribution approaches to Lorentzian Kappa distribution [25] while at $r = 0$ and $\kappa \to \infty$, this distribution approaches to Maxwellian distribution function [15]. We have plotted the growth rate of instability versus q giving different values to r. The plots of $\omega_{i\,\max}/\omega_{p1}$ versus q are plotted in figures 2, 3 and 4 for different n_1/n_2 ratios against fixed T_1/T_2 considering $r = 0,\ 1,\ 2$. figure 2 shows r $= 0$, figure 3 shows r $= 1$ and figure 4 reveals the truth for r $= 2$.

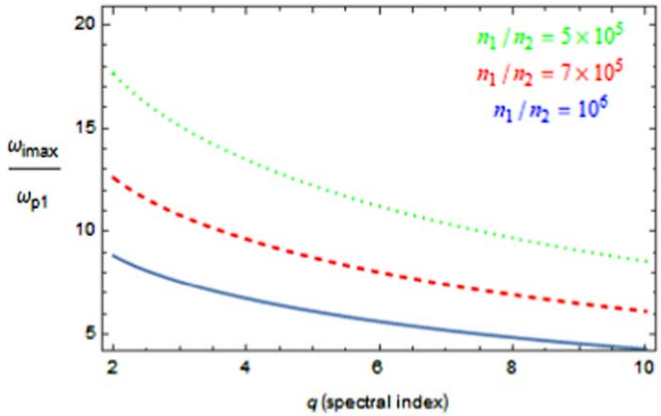

Figure 3. The Growth rate vs q (spectral index)for $n_1/n_2 = 5 \times 10^5, 7 \times 10^5, 10^6$ and $T_1/T_2 = 500$ where $r = 1$.

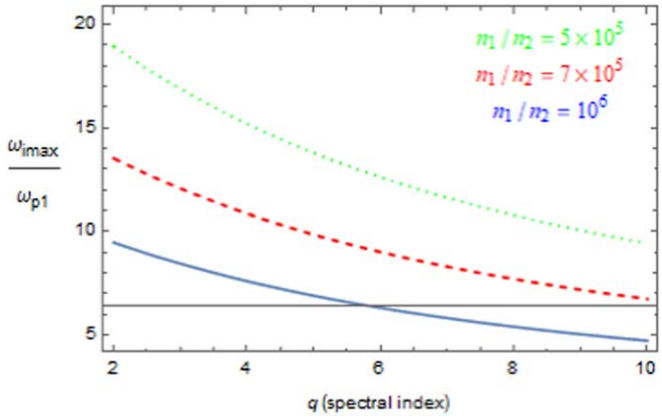

Figure 4. The Growth rate vs q (spectral index) for $n_1/n_2 = 5 \times 10^5, 7 \times 10^5, 10^6$ and $T_1/T_2 = 500$ where $r = 2$.

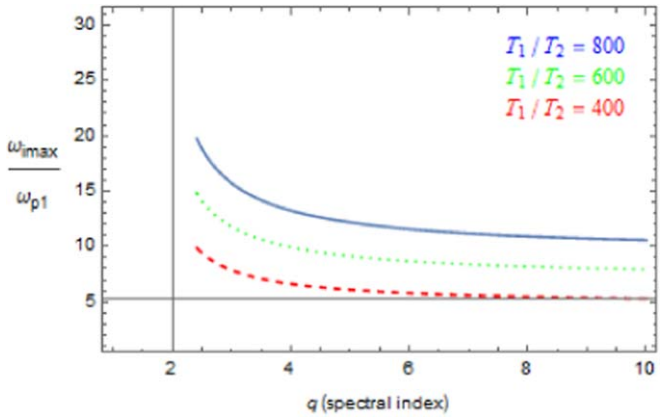

Figure 5. The Growth rate vs q (spectral index) for $T_1/T_2 = 800, 600, 400$ and $n_1/n_2 = 10^6$ where r = 0.

Similarly, figures 5, 6 and 7 are plotted for $\omega_{i\,\max}/\omega_{p1}$ versus q for different T_1/T_2 ratios against fixed n_1/n_2 considering $r = 0,\ 1,\ 2$, respectively. As the value of q increases, the growth rate decreases and starts approaching the value attained by Maxwellian distribution function [21].

Figures 2, 3 and 4 reveals that the growth rate is greater for small value of density ratio n_1/n_2 for fixed T_1/T_2 for $r = 0, 1, 2$ respectively. Figures 5, 6 and 7 represents that growth rate is higher at high value of T_1/T_2 at fixed n_1/n_2 for $r = 0, 1, 2$.

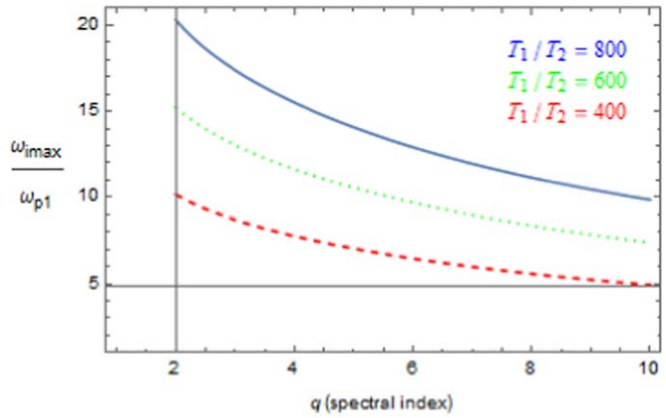

Figure 6. The Growth rate vs q (spectral index) for $T_1/T_2 = 800, 600, 400$ and $n_1/n_2 = 10^6$ where $r = 1$.

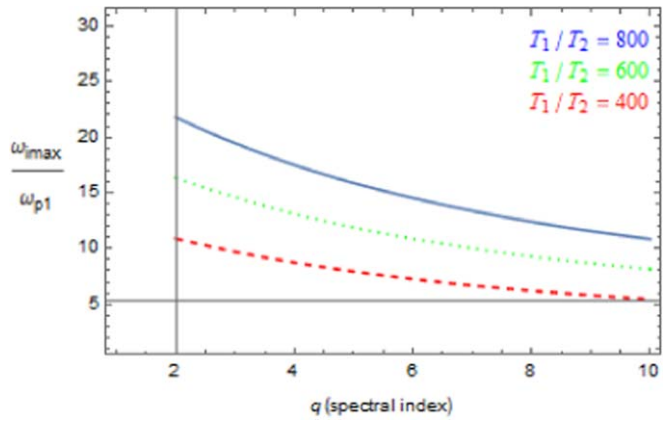

Figure 7. The Growth rate vs q (spectral index) for $T_1/T_2 = 800, 600, 400$ and $n_1/n_2 = 10^6$ where $r = 2$.

The spectral indices r and q generally represents the shoulder and the high energy tail of the distribution function respectively. It is evident from the figures 2 and 5 that for $r = 0$ and larger values of q the (r, q) distribution approaches the Maxwellian behavior. In both figures the ratios n_1/n_2 and $T_1/T_2$are kept constant alternatively.

When the value of r is increased i.e; $r = 1$, keeping q fixed in figures 3 and 6, with ratios n_1/n_2 and T_1/T_2 alternatively kept constant, the shoulder of the distribution function begins to form which represents the flat part of the distribution. The maximum growth rate of instability increases at larger r and smaller q representing the presence of larger number of superthermal electrons. But as the value of q increases, the growth rate of instability decreases due to decrease in the number of superthermal electrons. Consequently, energy transfer from the electrons to the wave decreases.

When the value of r is further increased i.e; $r = 2$, keeping q fixed in figures 4 and 7, the flat portion becomes more prominent. Again, n_1/n_2 and T_1/T_2 are kept constant respectively. This flattening of the tail also indicates that the lager number of particles are receiving energy from the wave as compared to particles giving energy to the wave thus leading to the decrease in the growth rate of instability at larger value of q. However, by increasing r with fixed value of q the maximum growth rate increases.

Figures 2, 3 and 4 at $r = 0$,1 and 2 against fixed ratio of number density emphasizes the maximum growth rate of the instability for high value of the number density of the electrons in the bump. Similarly, figures 5, 6 and 7 at $r = 0$,1 and 2 against fixed ratio of temperature shows that the maximum growth rate of instability is lower when the temperature of the electrons in the bump is low.

4. Conclusion

In the present manuscript, we ensured a complete and systematic analysis of bump on tail instability by analyzing the dispersion relation of Langmuir waves characterized by (r, q) velocity distribution function with

spectral indices r and q. It is observed that the growth rate is maximum at higher r values which clearly indicates the presence of larger number of electrons. It decreases with the increase in the value of q and approaches to its Maxwellian value. The wave particle interaction becomes significant at smaller q values. At smaller values of q, the electrons import more energy to the Langmuir wave thereby increasing the growth rate of the instability. With the decrease in the number of electrons at higher q values, the energy transfer from particles to wave is also decreased leading to the decrease in the growth rate of instability. With all these observations it can be concluded that the number density and temperature plays a significant role in the growth rate of instability. The maximum growth rate increases with increasing number density and decreases with the increasing temperature of electrons in the bump.

ORCID iDs

N Noreen https://orcid.org/0000-0002-4239-5616
A Shiekh https://orcid.org/0000-0002-6404-901X

References

[1] Filbert P C and Kellogg P J 1979 *J. Geophys. Res.* **84** 1369
[2] Papadopoulos K, Goldstein M L and Smith R A 1974 *Astrophys. J.* **190** 175
[3] Freund H P, Smith R A and Papadopoulos K 1981 *Phys. Fluids* **24** 442
[4] Klimas A J and Fitzenreiter R J 1988 *J. Geophys. Res.* **93** 9628
[5] Fitzenreiter R J, Klimas A J and Scudder J D 1985 *Geophys. Res. Letters* **11** 496
[6] Schmit P F, Mooney C R, Dodin I Y and Fisch N J 2011 *J. Plasma Phys.* **18** 042103
[7] Valentini F, Marco R D, Carbone V and Veltri P 2008 *Lett. J. Exploring* **83** 55001
[8] Zouganelis I 2008 *J. Geophys. Res.* **113** 08111
[9] Vasyliunas V M 1968 *J. Geophys. Res.* **73** 2839
[10] Summers D and Thorne R M 1991 *Phys. Fluids.* **03** 1835
[11] Zaheer S, Murtaza G and Shah H A 2004 *Phys. Plasmas* **11** 2246
[12] Zaheer S and Murtaza G 2007 *Phys. Plasmas* **14** 022108
[13] Zaheer S and Yoon P H 2013 *Astrophys. J.* **775** 108
[14] Qureshi M N S, Nasir W, Masood W, Yoon P H, Shah H A and Schwartz S J 2014 *Geophys. Res. Space Science* **119** 10059
[15] Krall N A and Trivelpiece A W 1973 *Principles of Plasma Physics* (New York: McGraw-Hill) 458
[16] Qureshi M N S, Pallocchia S G and Burno R 2003 *Solar Wind Ten AIP Conf. Proc. AIP, Melville* 679
[17] Krapchev V B and Ram A K 1980 *Phys. Rev.* **22** 1229
[18] Qureshi M N S, Shah H A, Murtaza G, Schwartz S J and Mahmood F 2004 *Phys. Plasmas* **11** 3819
[19] Qureshi M N S and Shi J K 2005 *Phys. Plasmas* **12** 122902
[20] Hashemzadeh M 2020 *Phys. Rev.* E **101** 013202
[21] Bittencourt J A 2004 *Fundamentals of Plasma Physics* (New York: Springer Verlag) (https://doi.org/10.1007/978-1-4757-4030-1)
[22] Issautier K, Chat G L, Meyer-Vernet N, Moncuquet M, Hoang S, MacDowall R J and McComas D J 2008 *J. Geophys. Res. Lett.* **35** 19101
[23] Issautier K, Perche C, Hoang S, Lacombe C, Maksimovic M, Bougeret J L and Salem C 2005 *Adv. Space Res.* **35** 2141
[24] Bukhari S, Khan S A and Ali S 2018 *Contri. Plasma Phys.* **58** 838
[25] Sarkar S, Paul S and Denra R 2015 *Phys. Plasmas* **22** 102109